Soft Matter

Electrostriction-Based Orientation Control of Blue Phase I Liquid Crystal

Journal:	*Soft Matter*
Manuscript ID	SM-ART-02-2025-000118.R1
Article Type:	Paper
Date Submitted by the Author:	19-Mar-2025
Complete List of Authors:	Nishi, Kento; Osaka University Nakajima, Kazuma; Osaka University, Ozaki, Masanori; Osaka University, Department of Elect., Electron. and Info. Eng.

ARTICLE

Electrostriction-Based Orientation Control of Blue Phase I Liquid Crystal

Received 00th January 20xx,
Accepted 00th January 20xx

DOI: 10.1039/x0xx00000x

Kento Nishi, Kazuma Nakajima*, Masanori Ozaki

An electric field-based orientation method for blue phase (BP) liquid crystals (LCs) enables particularly high-quality orientation and determines the BPI orientation by applying an out-of-plane electric field in a planar alignment cell. However, the mechanism, including the role of field-induced phases like BPX in BPI lattice reorientation, remains unclear. This study systematically investigates the role of BPX in BPI reorientation under various electric field conditions and alignment layer characteristics. When an out-of-plane electric field was applied, the [110] axis of BPI aligned in the field direction, and the [001] axis aligned along the easy axis. Under an in-plane electric field, the [110] axis aligned parallel to the field, while the out-of-plane orientation depended on alignment treatments. These results reveal that BPI lattice reorientation is determined by the applied field direction and alignment layer characteristics, even when reorientation is mediated solely through BPX. This research offers insights into the BPI orientation dynamics and introduces a method for achieving precise orientation control with reduced field intensities, enhancing the potential for advanced BPLC device applications.

Introduction

Cholesteric blue phases (BPs) are liquid crystal (LC) phases that emerge within a narrow temperature range between the cholesteric (Ch) phase and the isotropic phase in LC materials with high helical twisting power.[1] BPs self-organize into three-dimensional periodic structures consisting of double-twist cylinders (DTCs) formed by LC directors. Based on the symmetry of the DTC arrangement, they are classified into three sub-phases: BPI (body-centered cubic), BPII (simple cubic), and BPIII (disordered).[2] Due to their unique structure, BPs exhibit properties such as optical isotropy, circularly polarized light reflection in the visible wavelength range,[3] and sub-millisecond electro-optical responses.[4,5] Despite these excellent properties, BPLC had not been studied for application for a long time because of its inherently narrow expression temperature. However, it has been reported that the expression temperature range of BPLC can be significantly extended by forming a polymer network in the BP disclination,[6,7] and the application of BPLC has been expanded by the polymer-stabilized BPs (PSBPs).[8,9] In particular, the excellent optical and electro-optical properties of BPLCs make them promising candidates for applications in displays,[9–12] phase modulators,[13–16] and tunable lasers.[17–19]

Since BPs are optically isotropic, the orientation of the BP lattice was not a primary focus in early research. However, recent reports on the anisotropy of the electro-optical Kerr effect[20] and the reduction of hysteresis by obtaining large domain sizes[21,22] have shown the importance of orientation control for BPLC device applications. To date, various methods have been proposed for BP orientation control, including the alignment treatment of the substrate surface,[23,24] thermal processes,[22,25] electric field application,[26,27] and use of substrates with nano- and micro-scale patterns.[28–31] Achieving precise orientation control remains challenging due to the complex orientation mechanism associated with the higher-order director arrangement of BPs. Understanding this mechanism, particularly its behavior during phase transitions, is crucial for developing effective orientation techniques.

One method of BP orientation control by the application of an electric field is BPI reorientation through a field-induced phase transition, as proposed by Cho et al.[27] In this method, an out-of-plane electric field is applied to the BPI to dissolve the helical structure and induce a nematic (N) phase, and then the BPI is reoriented through the Ch phase and BPX in the process of removing the electric field. By conducting this treatment in a planar alignment cell, the lattice orientation of the reoriented BPI is uniquely determined. While this method provides high controllability, it requires a high electric field to induce the N phase. To address this challenge and enable more precise orientation control, a deeper understanding of the underlying orientation mechanisms is necessary. However, the specific influence of each field-induced phase on BPI reorientation has not been fully elucidated.

In this study, we investigated the role of BPX in the electric-field-induced reorientation of BPI. Under various alignment treatments and electric field direction conditions, BPI was reoriented without ever dissolving its helical structure by applying an electric field to the transition up to BPX and then removing the electric field. The orientation of BPI and BPX were affected by applied field direction and surface alignment, and they were particularly ordered during the phase transition. The

Division of Electrical, Electronic, Informational Engineering, Graduate School of Engineering, Osaka University, 2-1 Yamada-oka, Suita, Osaka 565-0871, Japan

result reveals that BPI lattice orientation is determined by the applied field direction and alignment layer characteristics, even when reorientation is mediated solely through BPX. This study provides insight into the behavior of field-induced BPI-BPX and BPX-BPI phase transitions, enhancing our understanding of BP phase transitions and electrostriction.

Experiment

A BPLC material was prepared by mixing a small-molecule nematic LC material, 4-cyano-4'-n-pentyl-biphenyl (5CB, Merck), a fluorinated nematic LC material (MLC-6849-100, Merck), and a left-handed chiral dopant (S-5011, HCCH) in a weight ratio of 51.3:46.8:2.9. The phase transition temperatures of the BPLC materials are 46.5°C for Ch-BPI, 46.9°C for BPI-BPII, and 48.4°C for BPII-Iso.

In this study, we prepared sandwiched cells for the application of an in-plane electric field and an out-of-plane electric field. The in-plane field cells were fabricated by attaching a glass substrate with comb-shaped ITO electrode with 100 μm electrode spacing and 200 μm electrode strip width to a glass substrate without ITO, having a cell thickness of 3 μm. In contrast, the out-of-plane field cells were prepared by assembling a pair of ITO-coated glass substrates with a cell thickness of 6 μm. For each field condition, two types of cells with different alignment layers were prepared: one type is a homogeneous cell, in which polyimide film (AL1254, JSR) is coated and rubbed for horizontal alignment, and the other type is a homeotropic cell, coated with polyimide film (JALS-2096-R16, JSR) for vertical alignment.

The orientation of BPs was observed using polarized optical microscopy (POM) and Kossel pattern analysis. The POM images were captured in reflection mode using a polarized optical microscope (ECLIPSE LV100POL, Nikon) equipped with a CMOS camera (EOS Kiss X4, Canon). The Kossel patterns, which are conoscopic images, were observed using the POM with reflective lighting, a Bertrand lens, a 100× objective lens (L Plan 100, Nikon) with a numerical aperture (NA) of 0.8, and a bandpass filter (center wavelength λ = 440 nm, bandwidth Δλ = 10 nm). The observations were conducted at approximately 46.8°C, the temperature at which the BPI to BPX phase transition occurs when an electric field is applied.

Results and Discussion

Reorientation by out-of-plane electric field

Figure 1 illustrates the orientation states of each phase during the BPI-BPX and BPX-BPI phase transitions induced by the application and removal of an out-of-plane electric field in (a) a homogeneous cell and (b) a homeotropic cell. The electric field intensity was varied at a rate of 0.15 V/μm per minute during both the application and removal processes.

In the homogeneous cell shown in Figure 1(a), the BPI, obtained through a phase transition from the cholesteric (Ch) phase, exhibited the (100) plane parallel to the substrate with random azimuthal orientation (Figure 1(a, i)). Upon applying the electric field, the phase transitioned to BPX, where the [001] axis (*c*-axis) realigned in the out-of-plane direction. Additionally, although the azimuthal orientation was random in BPI, in BPX the [110] axis was oriented parallel to the easy axis, as indicated by the Kossel pattern in Figure 1(a, ii). Upon removal of the electric field, the BPI showed a uniform orientation, with the (110) plane parallel to the substrate and the [001] axis parallel to the in-plane easy axis (Figure 1(a, iii)). Here, BPX is the tetragonal symmetry, and the length of each side is related to $a = b \neq c$, and the crystal axis $[abc]$ is defined correspondingly. The crystal axis of BPX is not the same as that of BPI due to different symmetry, and the BPX [001] axis corresponds to the BPI [110] axis elongated by the electric field.

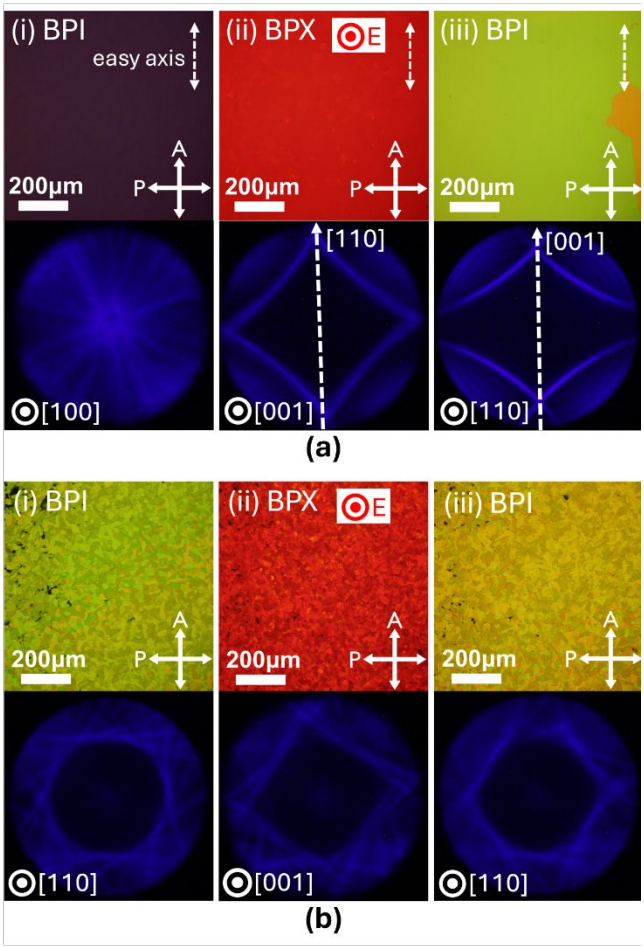

Figure 1 POM images and Kossel patterns of (i) BPI before applying out-of-plane field, (ii) BPX and (iii) BPI after removing out-of-plane field in (a) a homogeneous cell and (b) a homeotropic cell.

In contrast, in the homeotropic cell shown in Figure 1(b), the BPI was obtained by cooling from the isotropic phase, resulting in the (110) plane parallel to the substrate with random azimuthal orientation as the initial condition (Figure 1(b, i)). In the BPX induced by the application of the electric field, the [001] axis was aligned in the out-of-plane direction as in the homogeneous cell, but the azimuthal orientation remained random (Figure 1(b, ii)). After removing the electric field, the BPI transitioned from BPX, maintaining the (110) plane parallel to

the substrate, but the azimuthal orientation was not uniquely defined (Figure 1(b, iii)).

The results from the homogeneous and homeotropic cells suggest that the *c*-axis of BPX and the [110] axis of BPI align parallel to the electric field and that the presence of an in-plane easy axis is a critical factor in determining the azimuthal orientation of BPX and BPI.

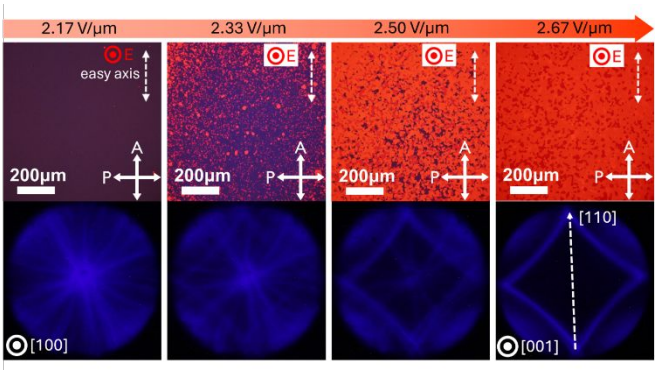

Figure 2 Sequential changes in POM images and Kossel patterns during BPI-BPX transition induced by applying out-of-plane field in a homogeneous cell.

As shown in Figure 1(a), the azimuthal orientation in the homogeneous cell becomes uniquely defined upon transitioning to BPX. Therefore, detailed observations of this phase transition were conducted, as illustrated in Figure 2. At 2.17 V/μm, the sample remained in the BPI phase just before the transition to BPX. From the Kossel pattern, the (100) plane was parallel to the substrate, and its azimuthal orientation remained random. This indicates that applying an out-of-plane electric field to the BPI with the (100) plane parallel to the substrate does not alter its orientation. At 2.33 V/μm, the phase transition began, and the four-fold symmetric Kossel lines of BPX appeared, overlapping with the randomly oriented Kossel lines of BPI. Additionally, it was evident that the azimuthal orientation of BPX became uniform immediately after the phase transition. As the electric field intensity increased further, the Kossel lines of BPI gradually disappeared, and at 2.67 V/μm, only the Kossel lines of BPX remained.

These sequential changes in the Kossel patterns demonstrate that the application of an electric field to BPI does not contribute to its orientation unless it undergoes a phase transition to BPX, but the phase transition to BPX induces a sudden change in orientation, achieving a uniquely defined azimuthal orientation. Regarding the BP orientation induced by temperature control, it has been reported that the phase transition usually starts near the substrate surface, and consequently the orientation state is strongly influenced by the surface condition of substrate.[32,33] Similarly, the field-induced phase transition may also start near the substrate surface, thereby strongly influencing the interface during the BPI-BPX phase transition and resulting in a uniform in-plane orientation of BPX along the easy axis.

Figure 3(a) shows the orientation behavior of BPI in a homogeneous cell during the process of reorientation by removing the out-of-plane electric field. At 2.00 V/μm, which corresponds to immediately after the BPX-BPI phase transition, a cross-hatched pattern characteristic of martensitic transformations,[34,35] which are diffusionless transformation. and associated with changes in lattice symmetry, was observed, and its magnified view is shown in Figure 3(b). Furthermore, its Kossel pattern is mirror-image symmetric with the Kossel pattern in (110) sharing one line, suggesting that it is twinned.[35-37] This can be attributed to the transition from body-centered tetragonal BPX to electrostricted BPI, where the [110] axis of BPI extends due to the out-of-plane electric field. From the Kossel pattern at 2.00 V/μm, two Kossel lines were observed, indicating that the (110) plane is parallel to the substrate and that there are two types of azimuthal orientations. This suggests the formation of twinning, a phenomenon where two crystal domains share a symmetrical orientation, due to structural changes during the phase transition.[36-38] However, from the Kossel pattern at 1.63 V/μm, only a single Kossel line indicating that the (110) plane is parallel to the substrate and the [001] axis is aligned parallel to the easy axis was observed. This orientation state remained unchanged even after the electric field was completely removed.

Furthermore, POM images and reflection spectra revealed that the reflection wavelength underwent discontinuous blue shifts during the electric field removal process. Two different colored domains are observed at 1.67 V/μm in the POM image in Figure 3a, and these two domains correspond to the two peaks at 1.67 V/μm in Figure 3c, where the peak on the longer wavelength side is the same as the peak wavelength at 2.0 V/μm. Thus, it indicates a discontinuous change in the interlayer distance, that is, a discontinuous change in the number of layers in the cell. When an electric field is applied along the [110] axis of BPI composed of LC materials with positive dielectric anisotropy, the lattice extends along the [110] direction.[39] Hence, removing the electric field increases the number of (110) layers along the cell thickness. Using Bragg's condition, the number of (110) layers in the out-of-plane direction was calculated from the measured peak wavelengths, and it was confirmed that the discontinuous change in the spectrum corresponds to a one-by-one increase in the number of layers. Fukuda reported by simulation that the number of (110) planes in a finite thickness cell of BPI takes discrete values.[40] Hence, the discontinuous spectral changes observed in this study (Figure 3(c)) are considered a manifestation of this predicted phenomenon.

Therefore, although BPI forms twinning immediately after the phase transition and the number of (110) layers increase with field removal, its final orientation inherits that of BPX, with the [001] axis aligned parallel to the easy axis. However, considering the structural similarity between BPX and the electrostricted BPI, both cases where the [001] axis is parallel or perpendicular to the easy axis are theoretically possible, as shown in Figure 3(d). Similar to the BPI-BPX phase transition, the influence of the surface is believed to restrict the orientation to the case where the [001] axis is parallel to the easy axis in the BPX-BPI phase transition.

ARTICLE

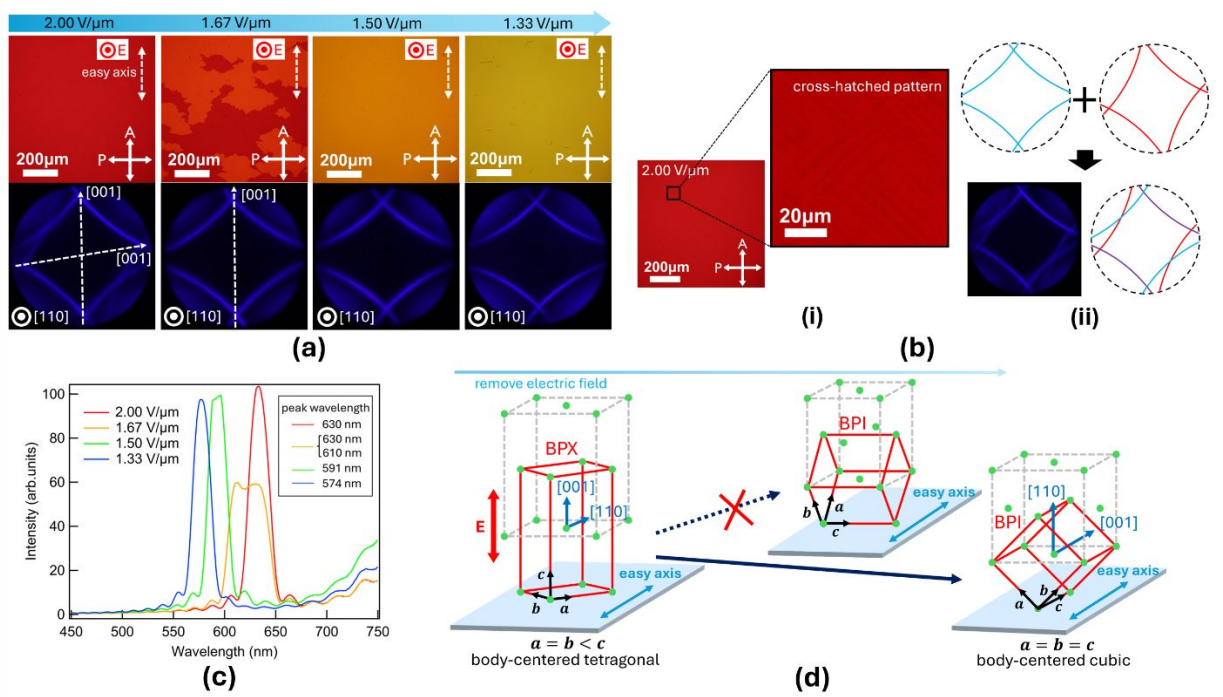

Figure 3 (a) POM images and Kossel patterns of BPI in a homogeneous cell during the process of reorientation by removing out-of-plane field. (b, i) Cross-hatch pattern of POM image and (b, ii) Kossel pattern indicating twinning of BPI, which appears immediately after the phase transition. (c) Reflected light intensity at each field intensity. (d) Schematic of BPs lattice orientation during BPX-BPI transition in out-of-plane field.

Reorientation by in-plane electric field

Figure 4 shows the orientation states of each phase in the BPI-BPX and BPX-BPI phase transitions induced by the application and removal of an in-plane electric field in (a) a homogeneous cell and (b) a homeotropic cell. During both the electric field application and removal processes, the electric field intensity was varied at a rate of 0.5 V/μm per minute. Here, the area shown in the POM images is only the inter-electrode area.

In the homogeneous cell shown in Figure 4(a), BPI obtained by cooling from the isotropic phase exhibited the (211) plane parallel to the substrate, with coexisting domains of azimuthal orientations differing by 180 degrees within the (211) plane. Using this initial condition, an in-plane electric field was applied to induce a transition to BPX. In Figure 4(a, ii), the POM image showed a blue texture, and the Kossel diagram showed a pattern where a circular pattern overlapped with a twofold symmetric pattern. This indicates that the [001] axis (*c*-axis) was parallel to the electric field and the [110] axis was aligned in the out-of-plane direction. When the electric field was then removed and the BPI was reoriented, the (001) plane was parallel to the substrate and the [110] axis aligned parallel to the electric field, as indicated by the Kossel pattern in Figure 4(a, iii). In the POM image, there are also green domains indicating the (110) plane, but the areas are too small to be reflected in the Kossel pattern.

In contrast, in the homeotropic cell shown in Figure 4(b), the initial condition for BPI was the same as shown in Figure 1(b), with the $(\bar{1}10)$ plane parallel to the substrate and random azimuthal orientations. In BPX, where the phase transition was induced by applying an in-plane electric field, the lattice orientation of BPX was consistent with that observed in the homogeneous cell, where the [001] axis aligned parallel to the electric field and the [110] axis aligned along the out-of-plane direction (Figure 4(b, ii)). However, after removing the electric field and transitioning back to BPI, the BPI exhibited the $(\bar{1}10)$ plane parallel to the substrate, with the [110] axis aligned parallel to the direction of the electric field (Figure 4(b, iii)).

The results from the homogeneous and homeotropic cells clearly demonstrate that the electric field aligns the [001] axis of BPX and the [110] axis of BPI parallel to the field direction, as illustrated schematically in Figure 4(c). Furthermore, it was revealed that BPX, aligned by the in-plane electric field, consistently exhibited the [110] axis aligned in the out-of-plane direction, regardless of the alignment layer used in the cell.

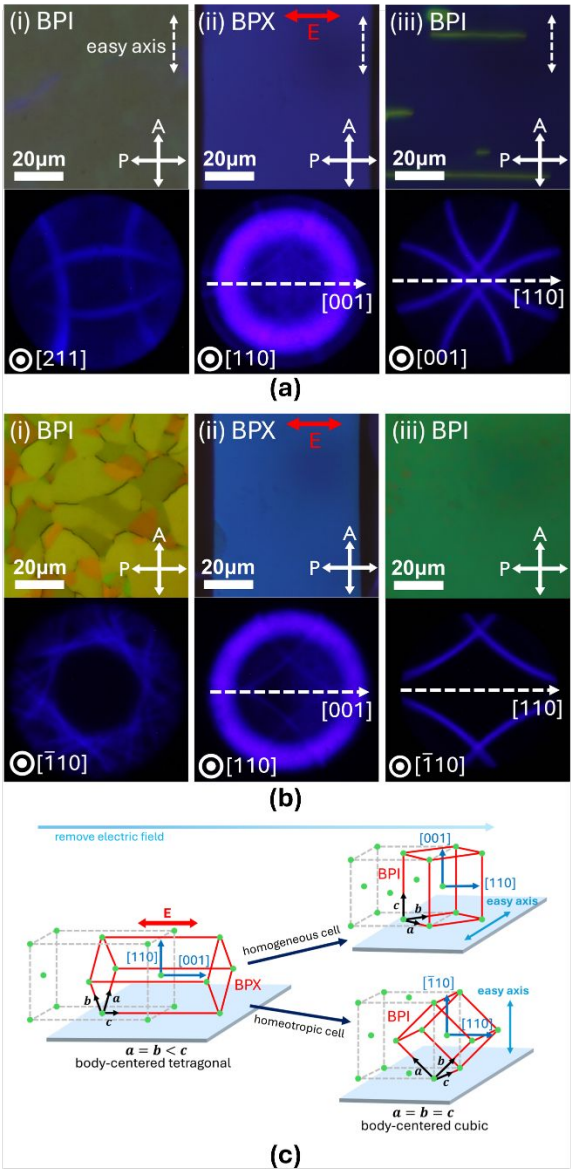

Figure 4 POM images and Kossel patterns of (i) BPI before applying in-plane field, (ii) BPX and (iii) BPI after removing in-plane field in (a) a homogeneous cell and (b) a homeotropic cell. (c) Schematic of BPs lattice orientation during BPX-BPI transition in in-plane field.

Figure 5 illustrates the behavior of the BPX-BPI phase transition during the in-plane electric field removal process in (a) a homogeneous cell and (b) a homeotropic cell. In the initial stage of the phase transition, a similar stripe-like texture was observed in both the homogeneous and homeotropic cells. This stripe pattern, formed parallel to the applied electric field, consisted of alternating dark blue and green regions. In the homogeneous cell, as the electric field was removed, the dark blue regions of the stripe pattern gradually expanded. In contrast, in the homeotropic cell shown in Figure 5(b), the green regions progressively expanded, accompanied by a subtle yet discontinuous shift from green to yellow-green in the reflection color, as indicated by the POM image at 2.5 V/μm. This discontinuous color shift is considered analogous to the phenomenon observed during the out-of-plane electric field removal process (Figure 3) and is attributed to the relaxation of BP lattice distortion induced by the in-plane electric field. This relaxation leads to lattice elongation along the out-of-plane direction[41] and a corresponding decrease in the number of ($\bar{1}$10) layers, as illustrated schematically in Figure 5(c).

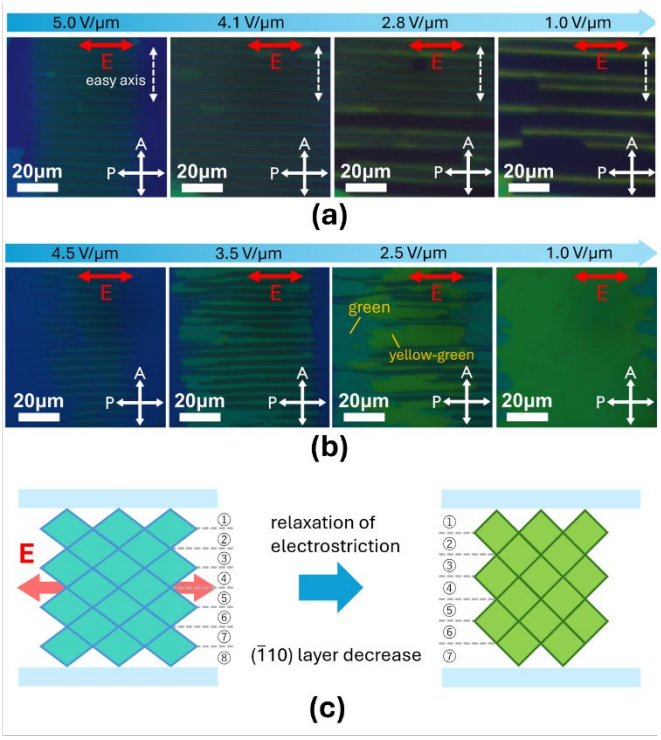

Figure 5 Sequential changes in POM images during BPX-BPI transition induced by removing in-plane field in (a) a homogeneous cell and (b) homeotropic cell. (c) Decrease in ($\bar{1}$10) layer due to relaxation of electrostriction.

The continuous expansion of the (001) plane region in the homogeneous cell and the ($\bar{1}$10) plane region in the homeotropic cell during the removal of the electric field suggests that the stripe pattern observed immediately after the transition from BPX was formed by the (001) and ($\bar{1}$10) planes of BPI. This suggests the formation of twinning due to structural changes during the phase transition as well as during the removal of the out-of-plane electric field. In the phase transition induced by the removal of the in-plane electric field, no influence of the substrate surface was observed. Although the substrate surface may affect the orientation even under the in-plane electric field condition, the specific effects of the surface are still unknown because the conditions for the BPI and BPX lattice planes in contact with the surface and the uniformity of the electric field are different from those under the out-of-plane electric field condition. However, it was evident that the interaction between the substrate surface and the molecules of BPI at the surface during the electric field removal process promoted a more stable orientation, resulting in a uniquely defined crystal plane parallel to the substrate. This finding underscores the significant role of the substrate surface in achieving stable and well-defined orientations during reorientation by electric field removal.

Conclusions

This study systematically investigated the effect of BPX on the electric-field-induced reorientation of BPI under various electric field application conditions and alignment layer configurations. Under the application of an out-of-plane electric field, BPI reoriented such that the [110] axis aligned with the out-of-plane direction and the [001] axis aligned along the easy axis. In contrast, with an in-plane electric field, the [110] axis aligned with the field direction, while the crystal axis in the out-of-plane direction varied depending on the alignment layer. Specifically, the [001] axis was aligned out-of-plane in the homogeneous cell, whereas the $[\bar{1}10]$ axis was aligned out-of-plane in the homeotropic cell. These findings reveal that the lattice orientation of reoriented BPI is uniquely determined by the direction of the applied electric field and the properties of the substrate surface, even when reorientation occurs exclusively via BPX. Additionally, the study demonstrated that the alignment states of BPI are significantly influenced by surface characteristics during the electric-field-induced BPI-BPX and BPX-BPI phase transitions. Notably, during the BPX-BPI phase transition, cross-hatched textures characteristic of martensitic transformations were observed under out-of-plane electric fields, whereas twin-like textures were observed under in-plane electric fields. These observations indicate that while BPX represents an electrostricted state of BPI, it undergoes substantial structural changes during phase transitions. The findings of this research provide a deeper understanding of the alignment dynamics in BPI and establish a novel method for achieving orientation control with reduced electric field intensity. This method, which reduces the required electric field while maintaining the high orientation controllability of field reorientation, is a major advance in BPI orientation technology and paves the way for more efficient and precise orientation control in BPLC applications.

Author Contributions

K.N. conducted the experiments and wrote the manuscript in discussion with K.N. and M.O. supervised this study.

Conflicts of interest

There are no conflicts to declare.

Acknowledgements

This work was partly supported by MEXT KAKENHI (JP23H02038) and a Grant-in-Aid for JSPS Fellows (23KJ1507).

References

1 Wright, D. C.; Mermin, N. D. Crystalline Liquids: The Blue Phases. *Rev. Mod. Phys.* **1989**, *61*, 385–432. https://doi.org/10.1103/RevModPhys.61.385.

2 Jérôme, B.; Pieranski, P.; Godec, V.; Haran, G.; Germain, C. Determination of the blue phase II structure. *J. Phys. France* **1988,** *49*, 837-844. https://doi.org/10.1051/jphys:01988004905083700.

3 Yoshida, H.; Anucha, K.; Ogawa, Y.; Kawata, Y.; Ozaki, M.; Fukuda, J. I.; Kikuchi, H. Bragg Reflection Band Width and Optical Rotatory Dispersion of Cubic Blue-Phase Liquid Crystals. *Phys. Rev. E* **2016**, *94*, 1–8. https://doi.org/10.1103/PhysRevE.94.042703.

4 Hisakado, Y.; Kikuchi, H.; Nagamura, T.; Kajiyama, T. Large Electro-Optic Kerr Effect in Polymer-Stabilized Liquid-Crystalline Blue Phases. *Adv. Mater.* **2005**, *17*, 96–98. https://doi.org/10.1002/adma.200400639.

5 Kikuchi, H.; Higuchi, H.; Haseba, Y.; Iwata, T. Fast Electro-Optical Switching in Polymer-Stabilized Liquid Crystalline Blue Phases for Display Application. *SID Symp. Dig. Tech. Pap.* **2007**, *38*, 1737–1740. https://doi.org/10.1889/1.2785662.

6 Kikuchi, H.; Yokota, M.; Hisakado, Y.; Yang, H.; Kajiyama, T. Polymer-Stabilized Liquid Crystal Blue Phases. *Nat. Mater.* **2002**, *1* (1), 64–68. https://doi.org/10.1038/nmat712.

7 Fukuda, J. I. Stability of Cholesteric Blue Phases in the Presence of a Guest Component. *Phys. Rev. E - Stat. Nonlinear, Soft Matter Phys.* **2012**, *86* (4), 1–6. https://doi.org/10.1103/PhysRevE.86.041704.

8 Yan, J.; Rao, L.; Jiao, M.; Li, Y.; Cheng, H.-C.; Wu, S.-T. Polymer-Stabilized Optically Isotropic Liquid Crystals for next-Generation Display and Photonics Applications. *J. Mater. Chem.* **2011**, *21* (22), 7870. https://doi.org/10.1039/c1jm10711a.

9 Huang, Y.; Chen, H.; Tan, G.; Tobata, H.; Yamamoto, S.; Okabe, E.; Lan, Y.-F.; Tsai, C.-Y.; Wu, S.-T. Optimized Blue-Phase Liquid Crystal for Field-Sequential-Color Displays. *Opt. Mater. Express* **2017**, *7* (2), 641. https://doi.org/10.1364/OME.7.000641.

10 Sun, Y.; Li, Y.; Zhao, Y.; Li, P.; Ma, H. A Low Voltage and Continuous Viewing Angle Controllable Blue Phase Liquid Crystal Display. *J. Disp. Technol.* **2014**, *10*, 484–487. https://doi.org/10.1109/JDT.2014.2302811.

11 Kikuchi, H.; Haseba, Y.; Yamamoto, S.; Iwata, T.; Higuchi, H. Optically Isotropic Nano-Structured Liquid Crystal Composites for Display Applications. *SID Symp. Dig. Tech. Pap.* **2009**, *40*, 578. https://doi.org/10.1889/1.3256842.

12 Chen, H.; Lan, Y.; Tsai, C.; Wu, S. T. Low-Voltage Blue-Phase Liquid Crystal Display with Diamond-Shape Electrodes. *Liquid Crystals* **2017**, *44*, 1124–1130. https://doi.org/10.1080/02678292.2016.1264014.

13 Hyman, R. M.; Lorenz, A.; Morris, S. M.; Wilkinson, T. D. Polarization-Independent Phase Modulation Using a Blue-Phase Liquid Crystal over Silicon Device. *Appl. Opt.* **2014**, *53*, 6925. https://doi.org/10.1364/ao.53.006925.

14 Sun, C.; Lu, J. A Polarization-Independent Blue Phase Liquid Crystal on Silicon with Low Operation Voltage. *Sci. Rep.* **2019**, *9*, 1–6. https://doi.org/10.1038/s41598-019-53344-6.

15 Oton, E.; Netter, E.; Nakano, T.; Katayama-D, Y.; Inoue, F. Monodomain Blue Phase Liquid Crystal Layers for Phase Modulation. *Sci. Rep.* **2017**, *7*, 1–9. https://doi.org/10.1038/srep44575.

16 Peng, F.; Lee, Y.-H.; Luo, Z.; Wu, S.-T. Low Voltage Blue Phase Liquid Crystal for Spatial Light Modulators. *Opt. Lett.* **2015**, *40*, 5097. https://doi.org/10.1364/ol.40.005097.

17 Liao, R.; Zhan, X.; Xu, X.; Liu, Y.; Wang, F.; Luo, D. Spatially and Electrically Tunable Random Lasing Based on a Polymer-Stabilised Blue Phase Liquid Crystal-Wedged Cell. *Liq. Cryst.* **2020**, *47*, 715–722. https://doi.org/10.1080/02678292.2019.1673842.

18 Yokoyama, S.; Mashiko, S.; Kikuchi, H.; Uchida, K.; Nagamura, T. Laser Emission from a Polymer-Stabilized Liquid-Crystalline Blue Phase. *Adv. Mater.* **2006**, *18*, 48–51. https://doi.org/10.1002/adma.200501355.

19 Lin, J. De; Wang, T. Y.; Mo, T. S.; Huang, S. Y.; Lee, C. R. Wide-Band Spatially Tunable Photonic Bandgap in Visible Spectral Range and Laser Based on a Polymer Stabilized Blue Phase. *Sci. Rep.* **2016**, *6*, 1–9. https://doi.org/10.1038/srep30407.
20 Kawata, Y.; Yoshida, H.; Tanaka, S.; Konkanok, A.; Ozaki, M.; Kikuchi, H. Anisotropy of the Electro-Optic Kerr Effect in Polymer-Stabilized Blue Phases. *Phys. Rev. E - Stat. Nonlinear, Soft Matter Phys.* **2015**, *91*, 1–6. https://doi.org/10.1103/PhysRevE.91.022503.
21 Nayek, P.; Jeong, H.; Kang, S.; Lee, S. H.; Park, H.; Lee, H. J.; Kim, H. S.; Lee, G. Effect of the Grain Size on Hysteresis of Liquid-crystalline Blue Phase I. *J. Soc. Inf. Disp.* **2012**, *20*, 318–325. https://doi.org/10.1889/jsid20.6.318.
22 Chen, H.-S.; Lin, Y.-H.; Wu, C.-H.; Chen, M.; Hsu, H.-K. Hysteresis-Free Polymer-Stabilized Blue Phase Liquid Crystals Using Thermal Recycles. *Opt. Mater. Express* **2012**, *2*, 1149. https://doi.org/10.1364/ome.2.001149.
23 Takahashi, M.; Ohkawa, T.; Yoshida, H.; Fukuda, J. I.; Kikuchi, H.; Ozaki, M. Orientation of Liquid Crystalline Blue Phases on Unidirectionally Orienting Surfaces. *J. Phys. D. Appl. Phys.* **2018**, *51*. https://doi.org/10.1088/1361-6463/aaaa4b.
24 Otón, E.; Morawiak, P.; Gaładyk, K.; Otón, J. M.; Piecek, W. Fast Self-Assembly of Macroscopic Blue Phase 3D Photonic Crystals. *Opt. Express* **2020**, *28*, 18202. https://doi.org/10.1364/oe.393197.
25 Chen, C. W.; Hou, C. T.; Li, C. C.; Jau, H. C.; Wang, C. T.; Hong, C. L.; Guo, D. Y.; Wang, C. Y.; Chiang, S. P.; Bunning, T. J.; Khoo, I. C.; Lin, T. H. Large Three-Dimensional Photonic Crystals Based on Monocrystalline Liquid Crystal Blue Phases. *Nat. Commun.* **2017**, *8*. https://doi.org/10.1038/s41467-017-00822-y.
26 Chen, Y.; Xu, D.; Wu, S. T.; Yamamoto, S. I.; Haseba, Y. A Low Voltage and Submillisecond-Response Polymer-Stabilized Blue Phase Liquid Crystal. *Appl. Phys. Lett.* **2013**, *102*. https://doi.org/10.1063/1.4802090.
27 Cho, S. Y.; Takahashi, M.; Fukuda, J. ichi; Yoshida, H.; Ozaki, M. Directed Self-Assembly of Soft 3D Photonic Crystals for Holograms with Omnidirectional Circular-Polarization Selectivity. *Commun. Mater.* **2021**, *2*. https://doi.org/10.1038/s43246-021-00146-x.
28 Li, X.; Armas-Perez, J. C.; Martinez-Gonzalez, J. A.; Liu, X.; Xie, H.; Bishop, C.; Hernandez-Ortiz, J. P.; Zhang, R.; De Pablo, J. J.; Nealey, P. F. Directed Self-Assembly of Nematic Liquid Crystals on Chemically Patterned Surfaces: Morphological States and Transitions. *Soft Matter* **2016**, *12*, 8595–8605. https://doi.org/10.1039/c6sm01733a.
29 Martínez-González, J. A.; Li, X.; Sadati, M.; Zhou, Y.; Zhang, R.; Nealey, P. F.; De Pablo, J. J. Directed Self-Assembly of Liquid Crystalline Blue-Phases into Ideal Single-Crystals. *Nat. Commun.* **2017**, *8*. https://doi.org/10.1038/ncomms15854.
30 Liu, S.; Nys, I.; Neyts, K. Two-Step Photoalignment with High Resolution for the Alignment of Blue Phase Liquid Crystal. *Adv. Opt. Mater.* **2022**, *10* (17), 2200711. https://doi.org/10.1002/adom.202200711.
31 Nakajima, K.; Mitsuhashi, S.; Cho, S. Y.; Ozaki, M. Slanted Structure of Blue Phase II Self-Aligned on One-Dimensional Patterned Surfaces. *ACS Appl. Mater. Interfaces* **2023**, *15*, 40054–40061. https://doi.org/10.1021/acsami.3c07293.
32 Chen, P.-J.; Chen, M.; Ni, S.-Y.; Chen, H.-S.; Lin, Y.-H. Influence of Alignment Layers on Crystal Growth of Polymer-Stabilized Blue Phase Liquid Crystals. *Opt. Mater. Express* **2016**, *6*, 1003. https://doi.org/10.1364/ome.6.001003.
33 Nakajima, K.; Ozaki, M. Anisotropic Crystal Growth in Blue Phase I Transitioned from a Uniformly Oriented Cholesteric Phase. *Soft Matter* **2024**, *20*, 4072–4078. https://doi.org/10.1039/d4sm00289j.
34 Jin, H. M.; Li, X.; Dolan, J. A.; Joseph Kline, R.; Martínez-González, J. A.; Ren, J.; Zhou, C.; de Pablo, J. J.; Nealey, P. F. Soft Crystal Martensites: An in Situ Resonant Soft x-Ray Scattering Study of a Liquid Crystal Martensitic Transformation. *Sci. Adv.* **2020**, *6*, 1–10. https://doi.org/10.1126/sciadv.aay5986.
35 Li, X.; Martínez-González, J. A.; Hernández-Ortiz, J. P.; Ramírez-Hernández, A.; Zhou, Y.; Sadati, M.; Zhang, R.; Nealey, P. F.; de Pablo, J. J. Mesoscale Martensitic Transformation in Single Crystals of Topological Defects. *Proc. Natl. Acad. Sci.* **2017**, *114* (38), 10011–10016. https://doi.org/10.1073/pnas.1711207114.
36 Zhang, Y.; Yoshida, H.; Cho, S.; Fukuda, J.; Ozaki, M. In Situ Optical Characterization of Twinning in Liquid Crystalline Blue Phases. *ACS Appl. Mater. Interfaces* **2021**, *13* (30), 36130–36137. https://doi.org/10.1021/acsami.1c06873.
37 Zhang, Y.; Yoshida, H.; Chu, F.; Guo, Y. Q.; Yang, Z.; Ozaki, M.; Wang, Q. H. Three-Dimensional Lattice Deformation of Blue Phase Liquid Crystals under Electrostriction. *Soft Matter* **2022**, *18*, 3328–3334. https://doi.org/10.1039/d2sm00244b.
38 Zhang, Y.; Zheng, Z. G. Programmable Orientation of Blue Phase Soft Photonic Crystal. *Appl. Phys. Lett.* **2024**, *125*. https://doi.org/10.1063/5.0236609.
39 Heppke, G.; Jérôme, B.; Kitzerow, H.-S.; Pieranski, P. Electrostriction of the Cholesteric Blue Phases BPI and BPII in Mixtures with Positive Dielectric Anisotropy. *J. Phys.* **1989**, *50* (19), 2991–2998. https://doi.org/10.1051/jphys:0198900500190299100.
40 Fukuda, J. Simulation of a Cholesteric Blue Phase Cell with Large but Finite Thickness. *Front. Soft Matter* **2022**, *2*. https://doi.org/10.3389/frsfm.2022.1011618.
41 Chen, H.-Y.; Hsu, K.-C. Electrically Tunable and Reversible Selective Reflection Due to the Transition between Simple Cubic and Tetragonal Blue-Phase Liquid Crystals. *Liq. Cryst.* **2020**, *47* (9), 1330–1337. https://doi.org/10.1080/02678292.2019.1710868.

Data Availability Statement

Date: 2025-02-04

The data supporting this study are available within the article.

Kazuma Nakajima
Division of Electrical, Electronic and Infocommunications Engineering
Graduate School of Engineering, Osaka University
2-1 Yamadaoka, Suita, Osaka 565-0871, Japan
Tel: 06-6879-4837
E-mail: knakajima@opal.eei.eng.osaka-u.ac.jp